A double bottom simulating reflector in the western Ross Sea, Antarctica

Riccardo Geletti[1] and Martina Busetti[1]

Received 26 July 2010; revised 21 December 2010; accepted 12 January 2011; published 5 April 2011.

[1] We present seismic evidence of the presence of gas hydrates and free gas in Victoria Land Basin (western Ross Sea, Antarctica). The occurrence of gas hydrates is inferred from a bottom simulating reflector (BSR), the first identified in the Ross Sea area. The gas presence was analyzed through targeted reprocessing of the multichannel seismic reflection data (3000 m streamer, 120 channels, 60-fold) acquired in 1990 by the Italian R/V *OGS-Explora*. The seismic data were reprocessed in order to increase the signal-to-noise ratio by adopting a true-amplitude approach, allowing a subsequent amplitude variations with offset (AVO) analysis to extract information on both P and S wave reflectivity. Along a profile from the deeper basin to an intrabasin structural high, the BSR evolves into crosscutting reflectors (CCRs) and enhanced amplitude reflectors (EARs). Locally, another seismic event is interpreted to be a second BSR (BSR0), identified about 150 m below the first BSR and is possibly related to the presence of a mixture of gases comprising methane and hydrocarbons with heavier molecular weight and therefore associated with a deeper hydrate stability zone. The presence of faults controls the upward gas migration, connecting the free gas zone below the BSR and the mud volcanoes and pockmarks on the seafloor. The modeling of the hydrate equilibrium zone shows that the observed BSR/BSR0 could be stable at the present pressure-temperature conditions.

Citation: Geletti, R., and M. Busetti (2011), A double bottom simulating reflector in the western Ross Sea, Antarctica, *J. Geophys. Res.*, *116*, B04101, doi:10.1029/2010JB007864.

1. Introduction

[2] In this study, the reappraisal of vintage multichannel seismic (MCS) reflection profiles from the Victoria Land Basin (western Ross Sea, Antarctica), reveals a double bottom simulating reflector (BSR). The BSR is a subclass of crosscutting reflectors (CCRs) (e.g., flat spot, bright spot) often discordant with the local stratigraphic sequences and is related to geological processes that occur after sediment deposition. The phase-inverted BSR is a classical indicator of gas hydrates and was observed for the first time by *Markl et al.* [1970]. The main diagnostic characteristics of a BSR, indicating the base of a zone of hydrate-bearing sediments, are the following:

[3] 1. The BSR normally mimics the seafloor topography, often crosscutting the local stratigraphy as it follows the gas hydrate stability field that is controlled by hydrolithostatic pressure, the seawater temperature and the geothermal gradient [e.g., *Shipley et al.*, 1979].

[4] 2. A high-amplitude phase-inverted reflector, which is characterized by a strong negative acoustic impedance contrast at the interface between high-velocity hydrate-bearing sediments above and low-velocity gas-bearing sediments below (a seismic velocity inversion) [e.g., *Hyndman and Spence*, 1992; *Andreassen et al.*, 2000; *Carcione and Tinivella*, 2000; *Gei and Carcione*, 2003].

[5] 3. In the prestack seismic analyses of the BSR, the amplitude variations with offset (AVO) features can be an important indicator of free gas at this interface [e.g., *Ostrander*, 1984; *Carcione and Tinivella*, 2000]. A downward transition to sediment-containing free gas with a low Poisson ratio, from an overlying sediment with hydrate having a medium high Poisson ratio, should give negative reflection amplitudes that become larger with increasing offset [e.g., *Minshull and White*, 1989; *Minshull et al.*, 1994; *Andreassen et al.*, 1997].

[6] A BSR can also be caused by diagenesis of siliceous sediments (opal A/opal CT transformation). This diagenesis-related BSR results from the positive acoustic impedance contrast between two forms of opal of dissimilar density (increasing with depth). Hence, diagenesis-related BSR shows a positive polarity as the seafloor reflection event [*Hein et al.*, 1978; *Davies and Cartwright*, 2002], in contrast to the negative polarity associated with the hydrate-related BSR.

[7] A second difference between hydrate and diagenetic-based BSRs is their response to seawater depth. With increasing water depth, the diagenesis-related BSR has a constant depth below the seafloor or even decreasing subbottom depth due to the opal transition pressures occurring at shallower depths [e.g., *Bohrmann et al.*, 1994]. In contrast, the gas-hydrate-related BSR is characterized by an increase

[1]Istituto Nazionale di Oceanografia e di Geofisica Sperimentale, Sgonico, Italy.

0148-0227/11/2010JB007864

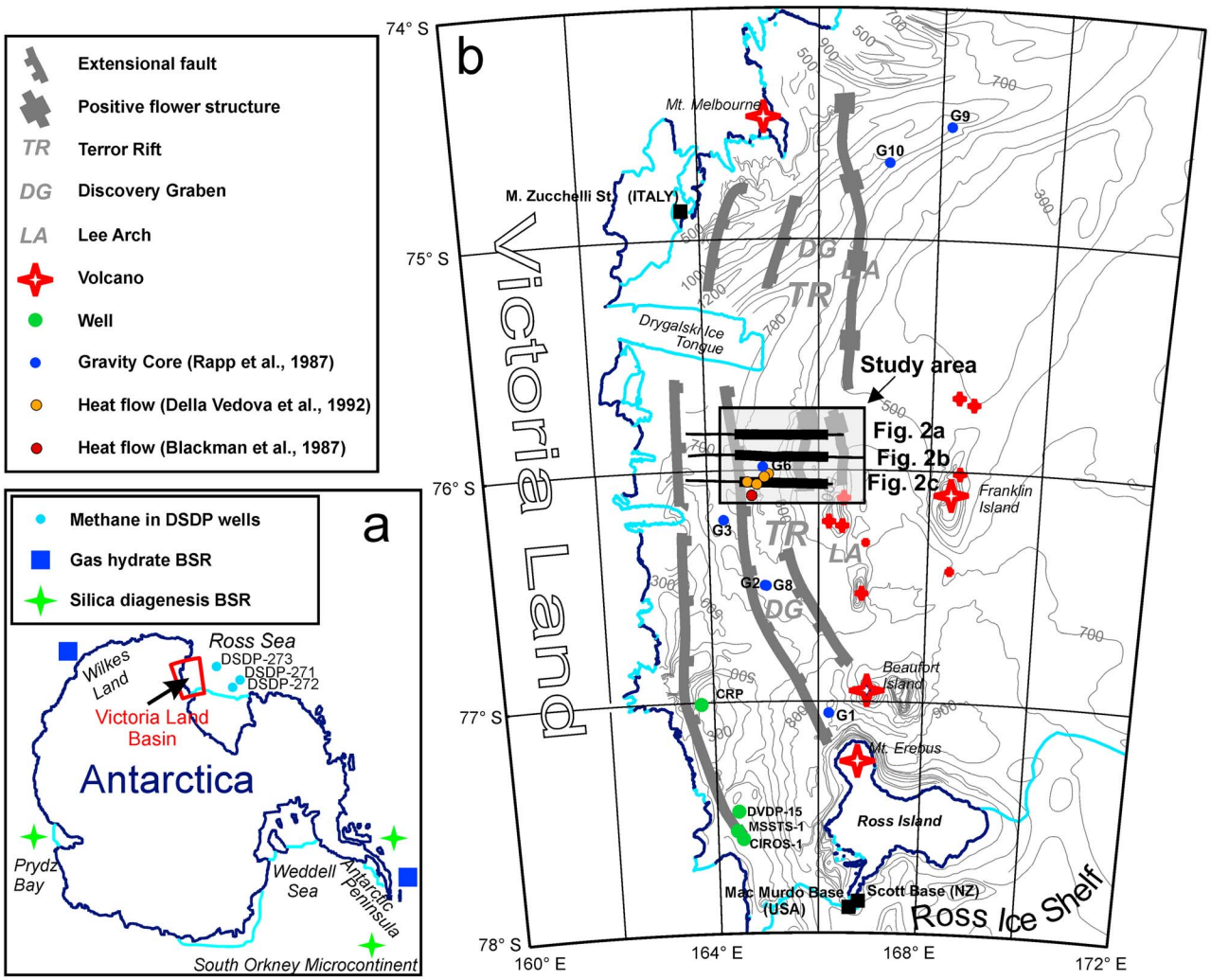

Figure 1. (a) The map of Antarctica shows the location of a bottom simulating reflector (BSR) correlated to the presence of gas hydrate at the continental rise of the offshore Wilkes Land [*Kvenvolden et al.*, 1987] and at the Antarctic Peninsula [*Lodolo et al.*, 1993] and to silica diagenesis at the continental rise of the Antarctic Peninsula [*Volpi et al.*, 2003], the South Orkney Microcontinent (SOM) [*Lonsdale*, 1990], and Prydz Bay [*Claypool et al.*, 2003; *Cooper and O'Brien*, 2004]. Evidence of hydrocarbon gases in the Ross Sea was reported by geochemical analyses in DSDP wells [*McIver*, 1975]. (b) Tectonic sketch map (modified after *Salvini et al.* [1997] and *Rossetti et al.* [2006]) and bathymetry (modified after *Davey* [2004]) of the western Ross Sea showing the position of the studied multichannel seismic profiles collected by OGS in 1990. Inside the Victoria Land Basin (VLB), the development of the north-south Terror Rift (TR) occurred due to the overprinting of the extensional phase by right-lateral strike-slip tectonics, with down faulting of the Discovery Graben (DG) and doming of the Lee Arch (LA) [*Cooper et al.*, 1987; *Salvini et al.*, 1997]. The recent magmatic activity of the McMurdo Volcanic Group is present both onshore and offshore in volcanic islands.

of depth below the seafloor with greater water depth, as the added pressure increases the hydrate stability temperature, allowing hydrate to be stable at greater, warmer depths [*Berndt et al.*, 2004].

[8] The gas hydrate-related BSRs are often accompanied by low-frequency events since the presence of free gas implies an absorption of the high-frequency components of the seismic energy [*Taylor et al.*, 2000; *Vanneste et al.*, 2002a]. Depending on the geology, the free gas may be localized in high-permeability layers, causing a discontinuous BSR defined by the abrupt termination of high-amplitude sedimentary reflections against an envelope that coincides with the theoretically expected depth of the base of the gas hydrate stability zone [*Berndt et al.*, 2004; *Bünz et al.*, 2003; *Mienert et al.*, 2001].

[9] Gas hydrates are present all over the world, however little is known about their occurrence offshore Antarctica (Figure 1a). BSRs, inferred to reveal the base of a zone of gas hydrate, were first identified in the continental rise of the offshore Wilkes Land [*Kvenvolden et al.*, 1987] and subsequently on the continental slope of the Antarctic Peninsula [*Lodolo et al.*, 1993], where the gas hydrate and

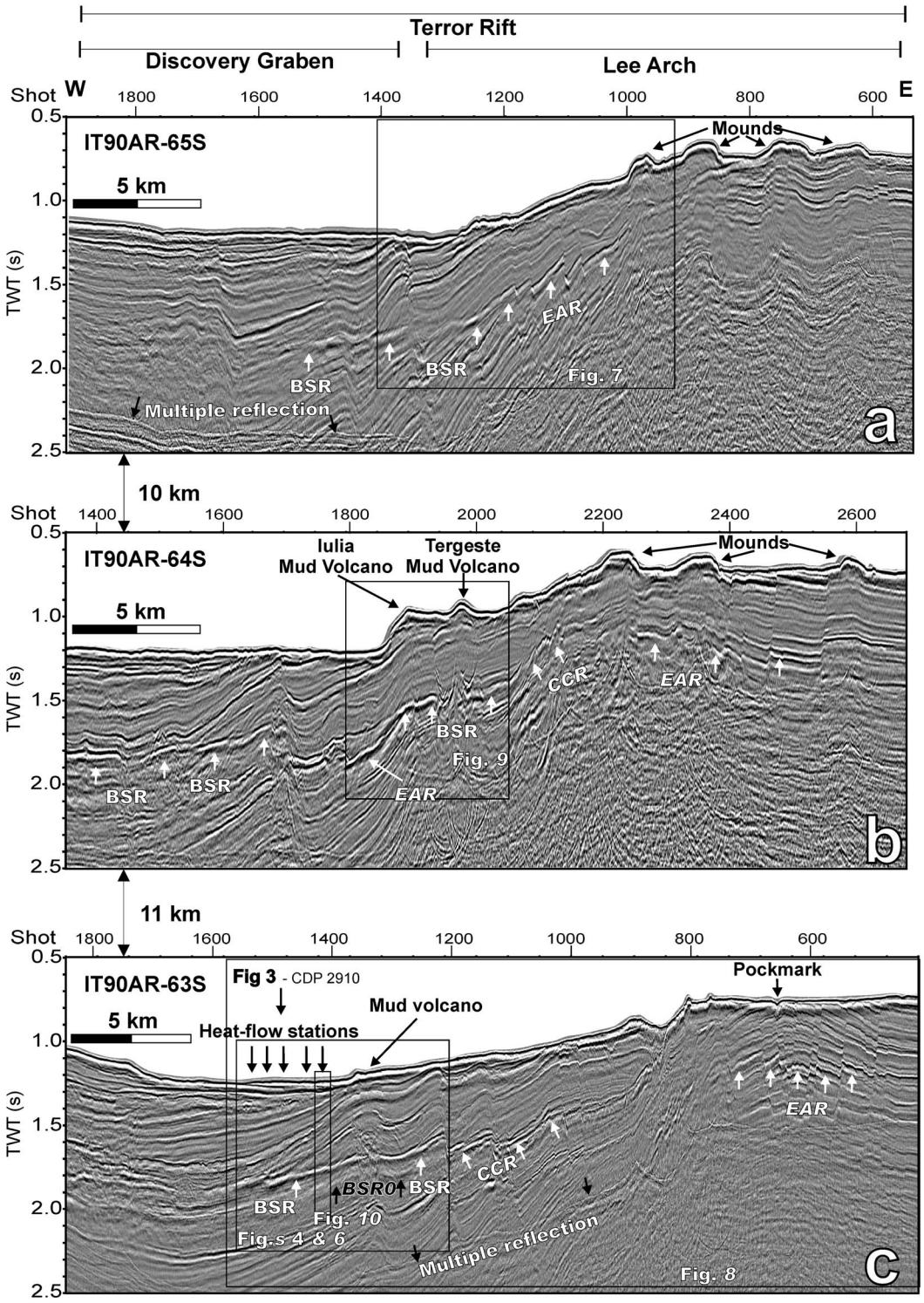

Figure 2. Reprocessed and migrated multichannel seismic profiles (a) IT90AR-65S, (b) IT90AR-64S, and (c) IT90AR-63S, collected by OGS in 1990 across the tectonically active Terror Rift in the Victoria Land Basin (see Figure 1 for location). The Terror Rift is subdivided into the Discovery Graben and the Lee Arch, both of which are affected by intense faulting and folding. Reprocessing of the profiles (see text) shows the bottom simulating reflector (BSR), crosscutting reflectors (CCRs), enhanced-amplitude reflectors (EARs), and a discontinuous BSR (BSR0). The seafloor morphology is characterized by mounds, mud volcanoes, and pockmarks.

free gas content has been extensively studied [*Tinivella et al.*, 1998; *Tinivella and Accaino*, 2000; *Lodolo et al.*, 2002]. However, BSR evidence in both areas appears on the continental rise in water depths ranging from 1000 to 4800 m. Offshore Antarctica, the occurrence of BSRs related to silica diagenesis, in particular, the diagenetic alteration of a biogenic opal–A to opal CT [*Kvenvolden and Cooper*, 1987], was found on the South Orkney Microcontinent [*Lonsdale*, 1990], in the sediment drifts of the continental rise of the Antarctic Peninsula [*Rebesco et al.*, 1997; *Volpi et al.*, 2003], and on the continental slope of Prydz Bay [*Claypool et al.*, 2003; *Cooper and O'Brien*, 2004]. Despite the fact that gas hydrate was not found in the Ross Sea, *McIver* [1975] and *Rapp et al.* [1987] hypothesized its occurrence.

[10] For the first time, this paper reports the presence of BSRs in the Ross Sea, occurring in the three east-west MCS profiles collected in 1990, in the central part of the Victoria Land Basin (VLB) (Figure 1b). We present seismic evidence of BSRs after detailed reprocessing to preserve true amplitude; this MCS data analysis clearly reveals a strong BSR and below it, a second BSR (BSR0) with normal polarity, which is not visible in data analyzed using standard processing.

[11] In some locations, as for instance in the Antarctic Peninsula [*Böhm et al.*, 1995], Barents Sea and Norwegian continental margin [*Andreassen et al.*, 1990, 2000], and Nankai slope [*Foucher et al.*, 2002], the presence of another BSR was identified below the Base of the Gas Hydrate Stability Zone (BGHSZ). Generally, this BSR is characterized by a normal-polarity reflection (not phase-reversed) slightly deeper than the BGHSZ. There are several hypothesis about BSR0: (1) A paleo-gas-hydrate BSR, i.e., an event originated from former pressure-temperature conditions [*Andreassen et al.*, 2000]; (2) a seismic event from the base of sediments partially saturated with gas hydrates containing a mixture of gases, i.e., a BSR with a different stability zone [*Andreassen et al.*, 2000]; (3) a reflection associated with mineral diagenesis [*Andreassen et al.*, 2000], as mentioned before; and (4) a residual BSR, which could be due to a recent migration of the BGHSZ, in response to recent sea bottom warming or tectonic uplift [*Foucher et al.*, 2002]. In the following, a tentative interpretation identifies the BSR0 with hypothesis 2, since we observe a similar velocity profile and signal polarity as in the work by *Andreassen et al.* [2000].

2. Regional Setting

[12] The Ross Sea is a large embayment on the Antarctica coastline, covering an area of about 750,000 km^2, with an average water depth of ~500 m. There are five north-south sedimentary basins in the Ross Sea, the Victoria Land Basin (VLB) being the westernmost basin (Figure 1). The VLB is ~150 km wide and 400 km long, and is estimated to contain up to 14 km of sediments [*Cooper et al.*, 1987; *Brancolini et al.*, 1995]. These sediments are Cenozoic fluvial/continental to marine deposits in origin, with occurrence of diamicton (very poorly sorted sediment deposited by glaciers in moraines) since the Miocene period, indicating an increase of glacial processes relative to climate cooling [*Cape Roberts Science Team*, 2000]. Since the Eocene, the extensional phase overprinted by right-lateral strike-slip tectonics produced, within the VLB, the north-south trending Terror Rift, that is composed of two parts, the down-faulted Discovery Graben and the adjacent magmatically intruded and folded Lee Arch [*Cooper et al.*, 1987; *Salvini et al.*, 1997].

Table 1. Acquisition Parameters of the Multichannel Seismic Profiles Analyzed in the Paper

Acquisition Parameters	Description or Value
Vessel	R/V *OGS-Explora*
Time period	1989/1990
Source type	Air guns (1 × 16 units) – 22.5 L
Operating pressure	140 bars (2000 psi)
Recording system	Sercel SN 358 DMX
Record length	6000 ms
Sampling rate	2 ms
Field filters	L.C., 8 Hz–18 dB/oct; H.C., 154 Hz–70 dB/oct
Group interval	25 m
Shot interval	25 m
Number of groups	120
Offset (source/first group)	150 m
Coverage	6000%
Streamer length	3000 m
Streamer depth	8 m
Source depth	6 m

[13] The study area is located in the central Terror Rift, the tectonically and magmatically active part of the VLB. In particular, the MCS profiles cross the faulted eastern side of the Discovery Graben and the transpressional features of the Lee Arch (Figures 1 and 2).

[14] The thermal conditions of the Ross Sea reflect the active continental-rifting environment, having high heat flow values, with a relative geothermal gradient of 76–123°C/km [*Della Vedova et al.*, 1992] and 98–108°C/km [*Blackman et al.*, 1987], measured in the upper 4 m of sediment in the Central VLB (Figures 1b and 2c). This higher geothermal gradient measured in shallow sediments in the Central VLB could be applicable to the upper sediment only. In fact, the geothermal gradients estimated in wells drilled in the southern VLB (Figure 1) have lower average values, ranging from 24 to 40°C/km, and usually a slightly non linear equilibrium gradient: 24°C/km in the 625 m below seafloor (mbsf) deep well CRP-2 [*Bücker et al.*, 2000], 28.5°C/km in the 870 mbsf deep well CRP-3 [*Cape Roberts Science Team*, 2000], 35°C/km in the 227 mbsf deep well MSSTS-1 [*Sissons*, 1980], 37°C/km in the 65 mbsf deep well DVDP 15 [*Bucher and Decker*, 1976], and 40°C/km in the 702 mbsf deep well CIROS-1 [*White*, 1989].

2.1. Hydrocarbon on the Continental Margins of the Ross Sea

[15] In the western Ross Sea, hydrocarbon gases and heavy η alkanes (ηC_{13} – ηC_{36}) were identified in near-surface sediments recovered by nine gravity cores (1–3 mbsf) (Figure 1b), but the low concentrations, for example, 9.6–13 μL/L of methane, were thought to reflect the background levels, commonly observed in the oxidizing sediment of continental margins [*Rapp et al.*, 1987]. Instead, in deeper Miocene muddy sediments (64–365 mbsf) recovered from DSDP sites 271, 272 and 273, in the eastern and northwestern part of the Ross Sea (Figure 1a), high

Table 2. Flow Chart of the Main Processing Sequence Applied to the Multichannel Seismic Profiles Analyzed in This Paper

Sequence	Description
1	Spherical divergence correction
2	Sort (60-fold common midpoints)
3	Preliminary velocity analysis
4	DMO correction procedure
5	Velocity analysis
6	NMO correction using optimum stacking velocities
7	Targeted top muting to include the far offset of the BSR events (maximum 35% of stretch)
8a	Stacking (fold 6000%)
8b	Extraction of AVO attributes
9a	Time migration using a smoothed version of the optimum stacking velocity field
9b	P and S wave reflectivity section

contents of total hydrocarbon gas (mainly methane), up to 179,000 μL/L, have been found [*McIver*, 1975]. Two gravity cores, collected near the DSDP-273, have methane concentrations from 3 to 6.7 μL/L, but concentrations in sediments at depth at DSPD-273 ranged from 52,000 to 146,000 μL/L, indicating that high methane content does not reach the sampled near-surface sediment [*Rapp et al.*, 1987]. Both *McIver* [1975] and *Rapp et al.* [1987] speculated that the gases may have been immobilized as gas hydrates, but at that time, evidence of clathrates or BSRs in seismic profiles was not observed. In the CIROS-1 well, the Oligocene to Miocene rocks contain small amount of organic carbon, hence little hydrocarbon potential, similar to those of MSSTS-1 (Figure 1b) [*Collen et al.*, 1989].

3. Reprocessing of the Multichannel Seismic Data

[16] An extensive multichannel seismic survey was conducted by the Istituto Nazionale di Oceanografia e di Geofisica Sperimentale (OGS), in the western part of the Ross Sea (Figure 1) during the 1989/1990 austral summer, and multibeam echosounder swath bathymetry data were also acquired by the OGS in 2006, both with the R/V *OGS-Explora* in the framework of the Italian Programma Nazionale di Ricerche in Antartide (PNRA).

[17] The acquisition parameters of the MCS reflection profiles (Table 1) were designed for the analysis of the seismic stratigraphy (middle resolution). The multichannel seismic reflection data were processed at OGS in 1992, using a standard processing flow and the main seismic sequences were interpreted by *Brancolini et al.* [1995].

[18] The present study is based on a reprocessing flow (Table 2) for characterizing BSRs, CCRs and EARs (Figure 2). The profiles were processed using the software packages

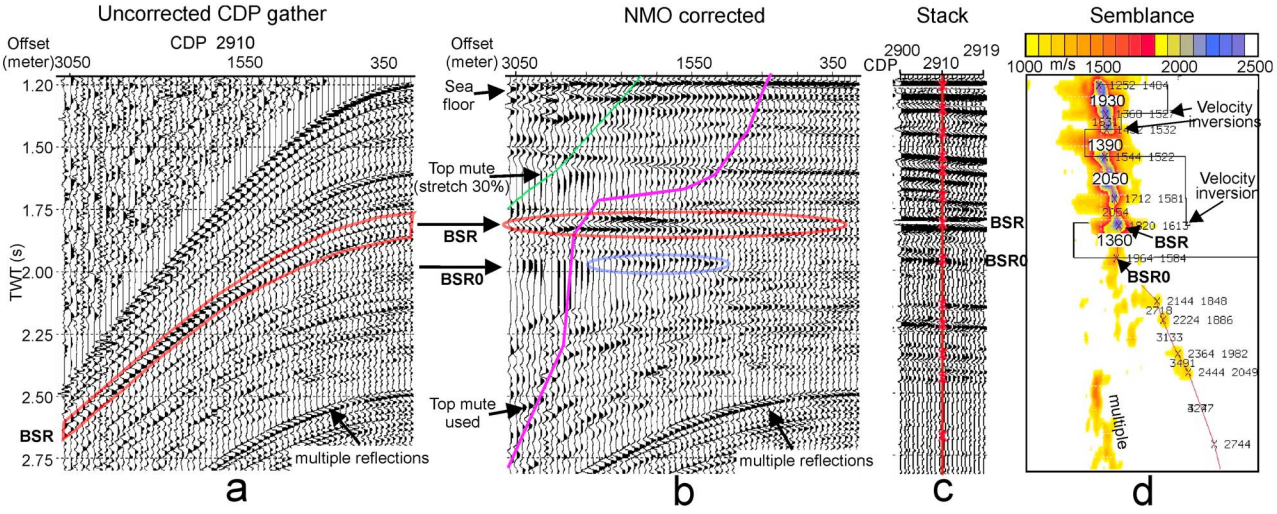

Figure 3. Common depth point (CDP) gather (2910) from profile IT90AR-63S (see location in Figure 2c): (a) 60-fold CDP 2910 gather after AGC and (b) after normal moveout (NMO) correction, where the strongest BSR is shown; (c) stack on 20 CDP around the CDP 2910; and (d) semblance velocity analysis and its relationship to the BSR/BSR0 pair. The semblance (low, yellow; high, blue) represents the coherence of the stacking velocity. The highest semblance peaks are picked to constitute the velocity function (red line) applied in the stacking process in Figure 3c. The interval velocity function is the segmented black line in Figure 3d. Numbers on the red line indicate interval velocity (V_i) and numeric pairs, such as 1432/1532, indicate the two-way traveltime (TWT) in ms and the root-mean-square velocity (V_{rms}), respectively, at the point indicated by the cross. In the CDP (Figures 3a and 3b), the BSR signals show an increase of negative amplitude with increasing offset, and the BSR0 signals are present only in the middle far-offset range. However, the BSR and BSR0 evidence in the stack profile is different according to the mute curve (magenta line in Figure 3b) and velocity functions used. The velocity inversions are present at 1360 and 1820 ms TWT, and the last one corresponds to the BSR with a velocity drop from 2050 to 1360 m/s. The shallower velocity drop is probably related to occurrence of free gas in the sediment below the mud volcano (see Figures 2c and 4). This may happen at locations where the mud volcano penetrates the gas hydrate layer, since faults may have caused a leak of a free gas to the seafloor.

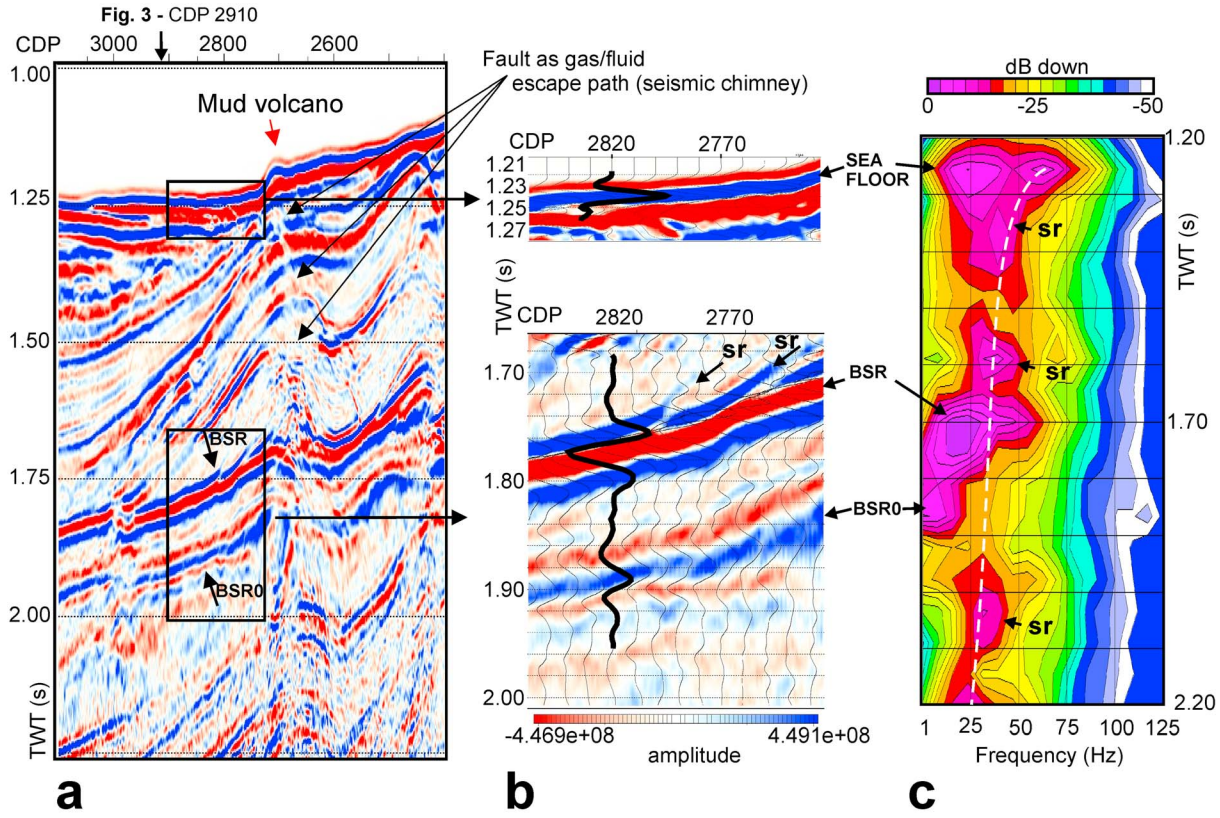

Figure 4. (a and b) The seismic character of the BSR and BSR0 compared to the seafloor reflection (see location in Figure 2c). The velocity trend in the sediment affects the polarity of the signal: the increase of interval velocity with time yields a normal polarity, while its decrease yields a negative polarity. The seafloor response has a positive polarity with the signal characterized by two negative lateral lobes and a main positive lobe (Figure 4b), as the sediment velocity at the seafloor (about 1650 m/s) is higher than that of water (~1480 m/s). A classical BSR is characterized by a negative polarity with two lateral positive lobes and a main negative lobe (Figure 4b), due to the drastically decreasing seismic velocity in the underlying layer, related to the gas presence. The negative polarity event (with respect to the seafloor), the velocity inversion and the crosscutting of the local stratigraphy (Figures 4a and 4b) are the main diagnostic characteristics of a BSR. The BSR0 has a normal polarity that could be caused by a thin layer of gas, with drop of velocity before it increases again, providing an overall reflection with a positive polarity rather than the reversed polarity of a standard BSR. (c) The frequency content of the three signals (seafloor, BSR and BSR0) is shown as a plot of power spectrum as a function of time [*Yilmaz*, 2001]: the seafloor has a wider spectrum, ranging from ~6 to ~75 Hz, with maximum amplitude at ~30 Hz, the BSR has the maximum amplitude at ~22 Hz, and the BSR0 has the maximum amplitude at ~15 Hz. SR refers to "stratigraphic reflectors," and the dashed white curve is the peak frequency trend versus TWT for water-saturated sediments (sediments without free gas).

Focus® and GeoDepth® by Paradigm®. The MCS acquisition geometry, such as the length of the streamer, the trace offset (the BSR events in the CDP gathers have the highest negative amplitudes range from 1500 to 2900 m along the offset; see Figures 3 and 5), the 6000% fold (spacing between CDPs is 12.5 m), and the frequency range and power of the source array allowed us to highlight the BSR features.

[19] The effects of geometrical spreading have been corrected by using the stacking velocities, and the relative amplitude of the seismic data has been preserved as well as possible in the prestack analysis, with accurate gain curve application to identify amplitude variations with offset. The true amplitude recovery is very important as it constitutes a diagnostic element for the BSR identification in the AVO analysis using the P and S wave reflectivities. A qualitative AVO analysis, hence an estimate of the S wave reflectivity image, was obtained with the commercial software GeoDepth®, which is based on a linearization of Zoeppritz's equations (Figure 6).

[20] An advanced stacking velocity analysis on each horizon of interest (i.e., the BSRs) including dip move out (DMO) correction was performed. The detailed velocity estimation was derived from semblance analysis with stack test sections of 30 CDP each (Figure 3) and applied every 30 CDPs (375 m), where the geological features are complex (Lee Arch) to 100 CDPs (1250 m) in the basin. The DMO brings the dipping events close to their real position [*Yilmaz*, 2001], hence emphasizing the BSR continuity

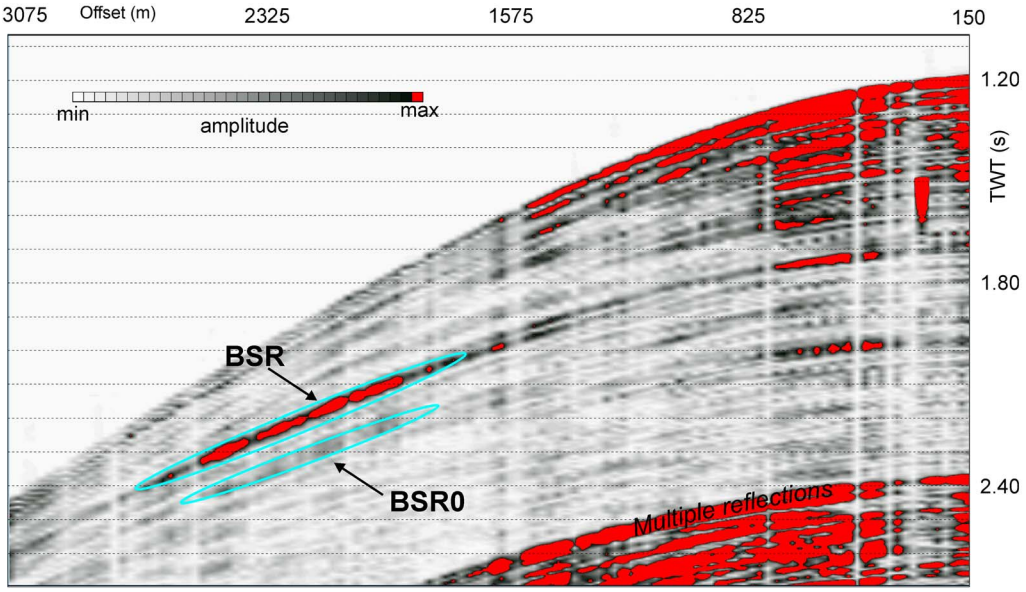

Figure 5. Absolute amplitude CDP gather obtained by a "true-amplitude" approach that preserves the real amplitudes of the reflection signals showing the high amplitude of the BSR at the far offset.

when crosscutting the geological features, and improving the determination of the velocity related to the BSR rather than the velocity of the stratigraphic horizons. In addition, we applied a targeted top muting, to preserve the shallow high-amplitude reflections (related to the BSR) occurring in the CDP gathers at offset between 1500 and 2900 m (Figure 3b).

[21] The dominant poststack frequency is 25–75 Hz, while the BSR signal has a main frequency of around 15 and 25 Hz (Figure 4c). The latter frequencies are anomalously low at this depth (down to 700 ms below the seafloor) compared to those of the stratigraphic reflectors (sr) at the same traveltime. The seismic source, 16 air guns with a frequency range between 10 to 120 Hz, was suitable to generate reflections from those interfaces.

[22] As mentioned above, the seismic data were reprocessed in order to increase the signal/noise ratio by adopting a "true-amplitude" approach, which preserved the real amplitudes of the reflection signals (Figure 5), allowing a successive AVO analysis and the calculation of the P and S wave reflectivity profiles (Figure 6) [*Stewart*, 1990].

[23] Complex seismic trace attributes, reflection strength (also known as instantaneous amplitude or envelope amplitude) and instantaneous frequency [*Taner and Sheriff*, 1977], were extracted to highlight the free gas occurrence (Figures 7 and 8). The reflection strength depends on the contrast of seismic impedance (i.e., velocity times density), and it is independent of the effects of phase distortion in the stacked seismic section. The seismic compressional (P wave) velocity decreases when there is gas filling the pores, even for small saturations [*Domenico*, 1977], and produces strong reflection events, called "bright spots." Hence, a high-reflection strength is often associated with gas accumulations [*Taner et al.*, 1979, 1994]. According to the principle that gas occurrence attenuates high frequencies [*Taner et al.*, 1979, 1994; *Carcione and Picotti*, 2006], the data were displayed as an instantaneous frequency section that produces a "low frequency shadow" over the region of inferred free gas (Figure 8b) [*Taylor et al.*, 2000, *Vanneste et al.*, 2002a].

4. Results

[24] Reprocessing the multichannel seismic data highlighted the occurrence, within the Miocene/Oligocene sediment, of four types of high-amplitude reflectors, with negative or positive polarity and low-frequency events associated with velocity anomalies. The four reflector types have been identified as follows:

[25] 1. BSR "proper," according to the definition of *Berndt et al.* [2004], is characterized by very high amplitudes, a phase inversion relative to the seafloor reflection event, and a tendency to parallel the seafloor topography while crosscutting the local seismic stratigraphy (Figures 2, 4, and 8). The BSR is present in the eastern side of the Discovery Graben only, and it is cut by faults. It occurs from 500 to 700 ms below the seafloor (~400–600 mbsf). Above the BSR, the interval velocities are about 1900–2050 m/s, and below it they drop to about 1360 to 1400 m/s. The main frequency of the BSR is about 20 Hz, lower than the 25 Hz of the stratigraphic reflectors occurring at the same time window (Figure 4c). In the prestack analysis, the negative amplitude of the reflectors increase with offset, as the negative main lobe of the signal has an amplitude approximately 10 times greater in the far offset (in particular between 1575 and 2825 m) than in the near offset (Figures 3 and 5). In the AVO analysis of the P and S wave reflectivity sections, the BSR shows high amplitude in the P wave section while is not evident in the S wave reflectivity (Figure 6).

[26] 2. A second BSR (BSR0), according to the interpretation of *Andreassen et al.* [2000], occurs as a reflection segment almost 200 ms (~150 m) below (and parallel to) the BSR but is characterized by an amplitude lower than that of the BSR and by a normal polarity. This event can

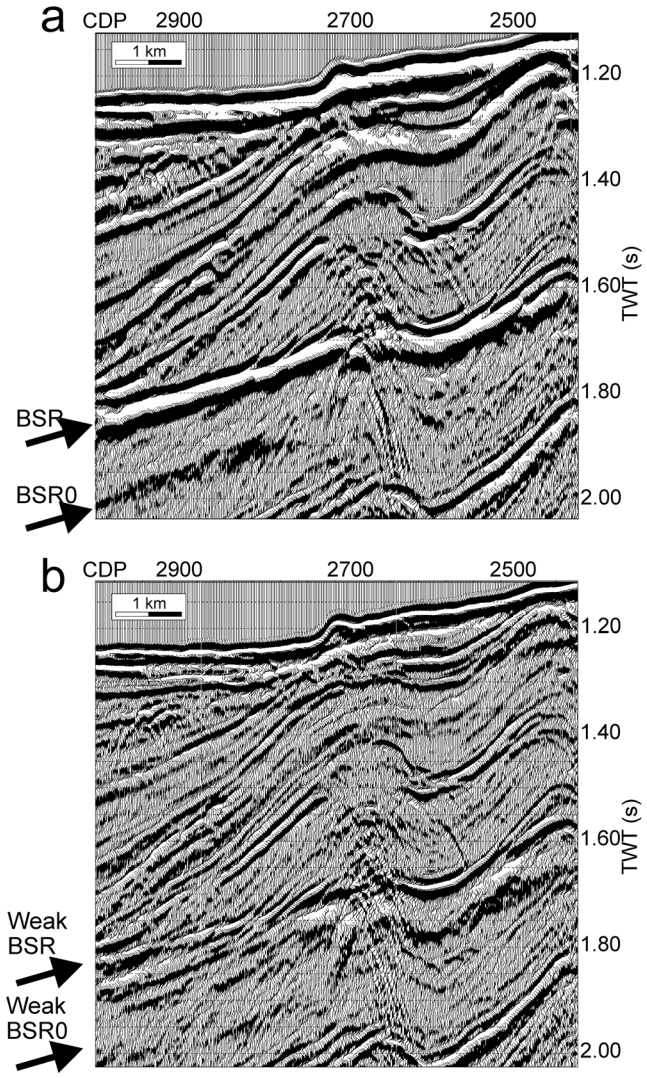

Figure 6. Part of line IT90AR-63S (see Figure 2 for location) corresponding to a gas-seeping feature and mud volcano: (a) P wave reflectivity section where the BSR/BSR0 are most evident in the whole study area. (b) S wave reflectivity section weakly images BSR/BSR0.

only be seen in the southern line in the Discovery Graben, where the BSR appears as the strongest event (Figure 2c). Above the BSR0, the interval velocities range from 1360 to 1400 m/s and below the BSR0 they increase to about 2000 to 2100 m/s. Qualitatively, this is a similar velocity profile to that reported by *Andreassen et al.* [2000]. The main frequency of the BSR0 is about 10–15 Hz, lower than that of the stratigraphic reflectors (25 Hz) occurring at the same time window (Figure 4).

[27] 3. Crosscutting reflectors (CCRs), according to the definition of *Berndt et al.* [2004], have the same seismic characteristics of the BSR proper, but they do not mimic the seafloor. They are present in the western side of the Lee Arch only in the southern profile (Figures 2c and 8a), rising up from 300 to 150 ms in correspondence with a 1.5 km wide depression in the seafloor. Above the CCRs the interval velocities are about 2000 m/s, and below they drop to about 1400 m/s (Figure 8a).

[28] 4. Enhanced-amplitude reflectors (EARs), according to the definition of *Judd and Hovland* [2007], are coherent seismic reflections. These high-amplitude reflections, which are related to the presence of gas, generally are characterized by high amplitude, reverse polarity and low frequency. They are present in the Lee Arch (Figure 2). The dominant frequency is about 22 Hz. Occasionally, the EARs are identified by a borderline top termination against the BSR (Figure 7).

[29] A wide and almost continuous area characterized by low frequencies, between 5 and 20 Hz, crosses the whole section roughly parallel to the seafloor, rising up and becoming thicker beneath the central portion of the Lee Arch. The distribution of the low frequencies, termed the "low frequency shadow," follows the distribution of the BSR, CCRs, and EARs (see Figure 8).

4.1. Fault and Gas Seep Induced Mud Volcano

[30] The area of BSR occurrence, particularly in the Lee Arch region, is affected by active tectonism. Fault strands disrupt the BSRs, the CCRs, and EARs, and are sometimes associated with mud volcanoes and pockmarks occurring at the seafloor (Figure 2). The main mud volcano, named Tergeste Mud Volcano, is 1000 m wide and 80 m high and located atop one strand belonging to the fault system of the Lee Arch (Figures 2b and 9). A smaller mud volcano is located in the Discovery Graben (Figure 2c). Both the BSR and the BSR0 underlie the mud volcanoes and are disrupted by faults just below the cones. Conduits rising up from the BSR to the mud volcanoes are visible in the seismic profiles (Figures 4 and 9), and are potentially related upward migration of gas/fluids.

[31] Moreover, beneath the Tergeste Mud Volcano the BSRs rise up almost 200 ms, and the thickness between the BSR and BSR0 of about 130 m (200 ms with low velocity values of about 1340 m/s) is the maximum observed in the study area.

4.2. Modeling of the Stability Zone of the BSR

[32] To evaluate whether the observed BSR and BSR0 represent the base of gas hydrate stability, the theoretical depth of the base of the gas hydrate stability zone was estimated for a range of methane hydrates and hydrates of varying composition [*Sloan*, 1990] (Figure 10). This model was performed on the part of seismic profile IT90AR-63S where the BSR and the BSR0 are strongest and the temperature measurements are available (Figures 1b and 2c) [*Della Vedova et al.*, 1992]. The average geothermal gradient is about 90°C/km, the seafloor temperature is about −1.5°C [*Della Vedova et al.*, 1992], and the water depth is 880 m. However, the geothermal gradient is not constant with depth, and is generally higher in the shallow sediment, so these values can be considered reliable for about the upper 50–100 mbsf (B. Della Vedova, personal communications, 2009). The geothermal gradient, calculated from hundred meter deep wells in southern VLB ranges only from 24 to 40°C/km. Assuming the BSR and BSR0 represent the base of stability of gas hydrate with different composition according the curve of *Sloan* [1990], with pure methane for BSR and heavier hydrocarbons (96% methane,

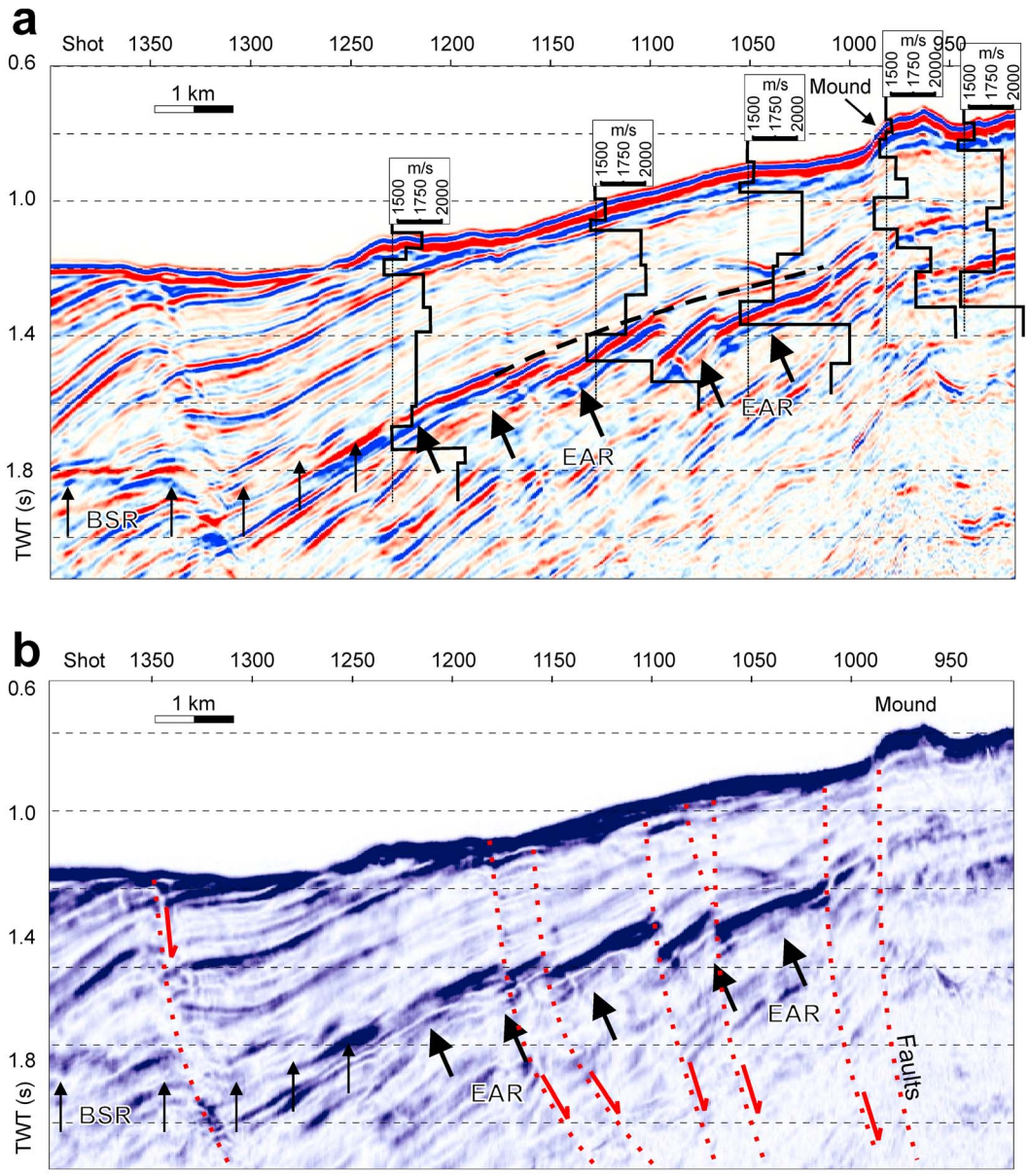

Figure 7. Migrated seismic section IT90AR-65S (a) with velocity functions and (b) the relative reflection strength section (see Figures 1 and 2a for location). The enhanced-amplitude reflections (EARs), disrupted by faults, show phase inversion in Figure 7a and high reflection strength in Figure 7b, and the velocity drop to about 1350 m/s provides evidence of a free gas zone. The dashed line is the borderline top of EARs termination that shows a bottom simulating trend and is the continuation of the BSR.

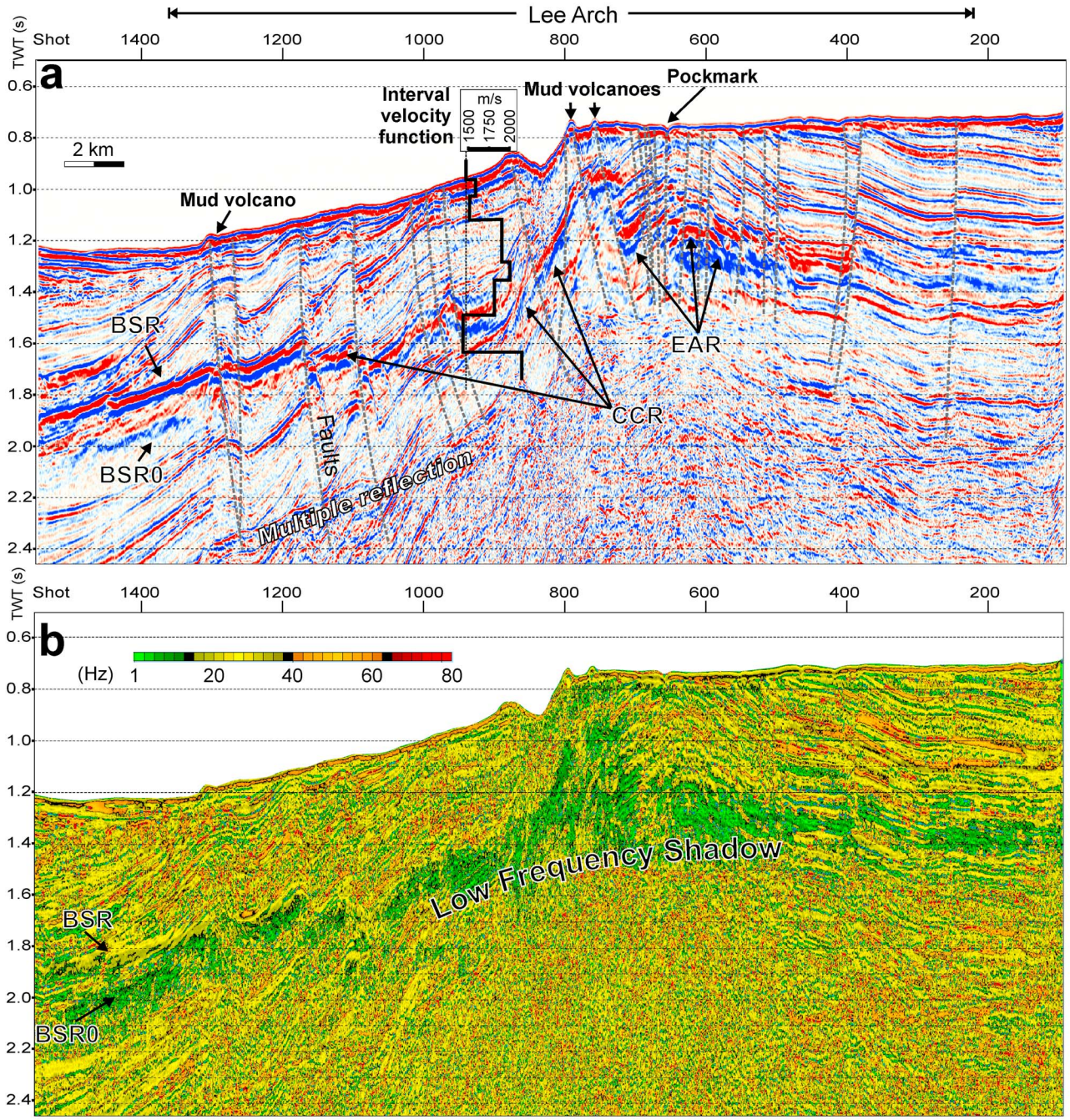

Figure 8. (a) Stack with true-amplitude approach and (b) instantaneous frequency section of IT90A-63S (see Figure 1 and 2c for location). In Figure 8a the BSR, crosscutting reflectors (CCRs), and enhanced-amplitude reflectors (EARs) are present. In the instantaneous frequency section a wide and almost continuous area characterized by low-frequency shadow (5–20 Hz), follows the distribution of the BSR, the CCRs, and EARs. The low frequency is an indicator of the free gas occurrence.

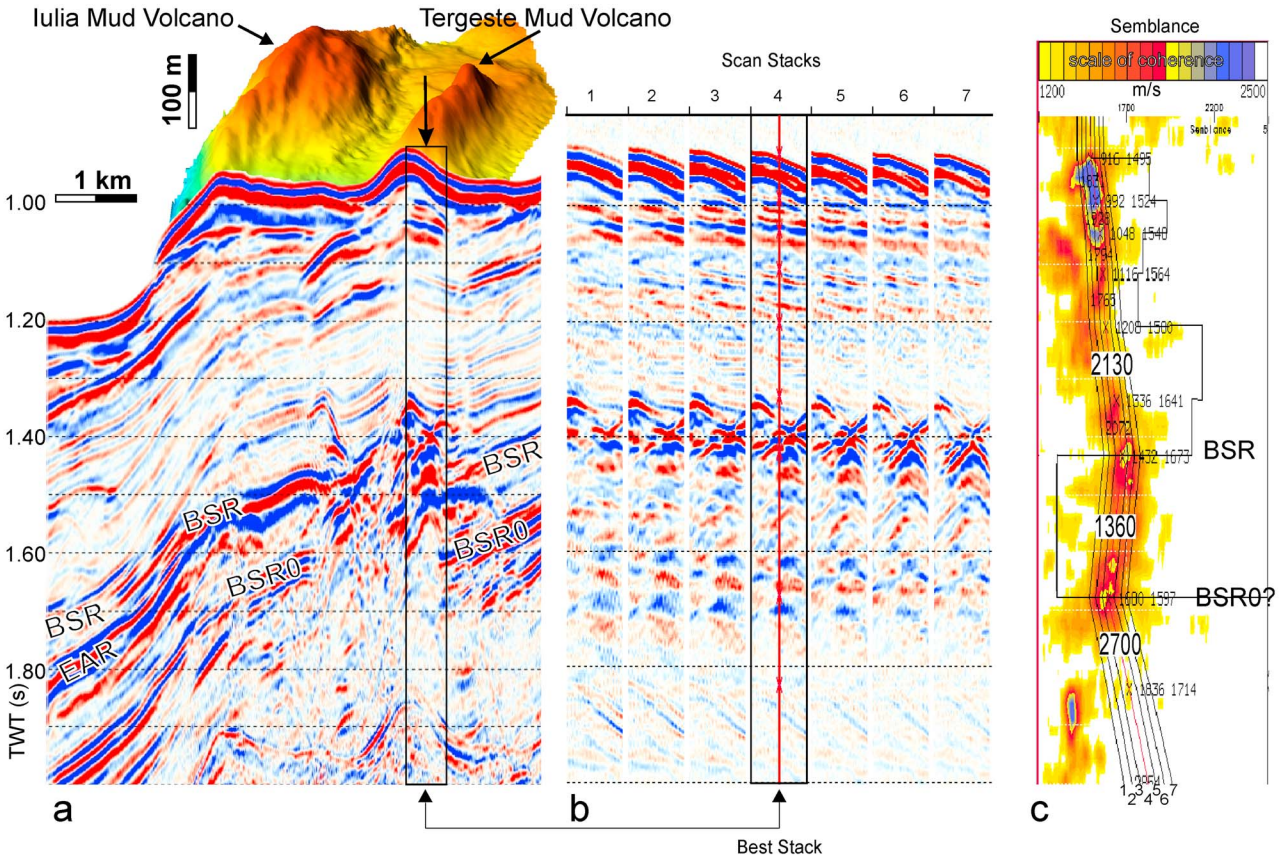

Figure 9. (a) A 3-D image of seismic migrated section IT90AR-64S (see location in Figure 2b) and multibeam echosounder swath bathymetry data across the Tergeste Mud Volcano. (b) Scan stacks and (c) relative semblance velocity analysis which highlight the seismic velocity inversion (1360 m/s between the BSR and BSR0) below the mud volcano. The thickness of this low-velocity zone is estimated to be ~170 m (250 ms). The BSR is intensively disrupted by faults, where gas, fluid, and fluidized sediments migrate upward, building the mud volcano at the seafloor.

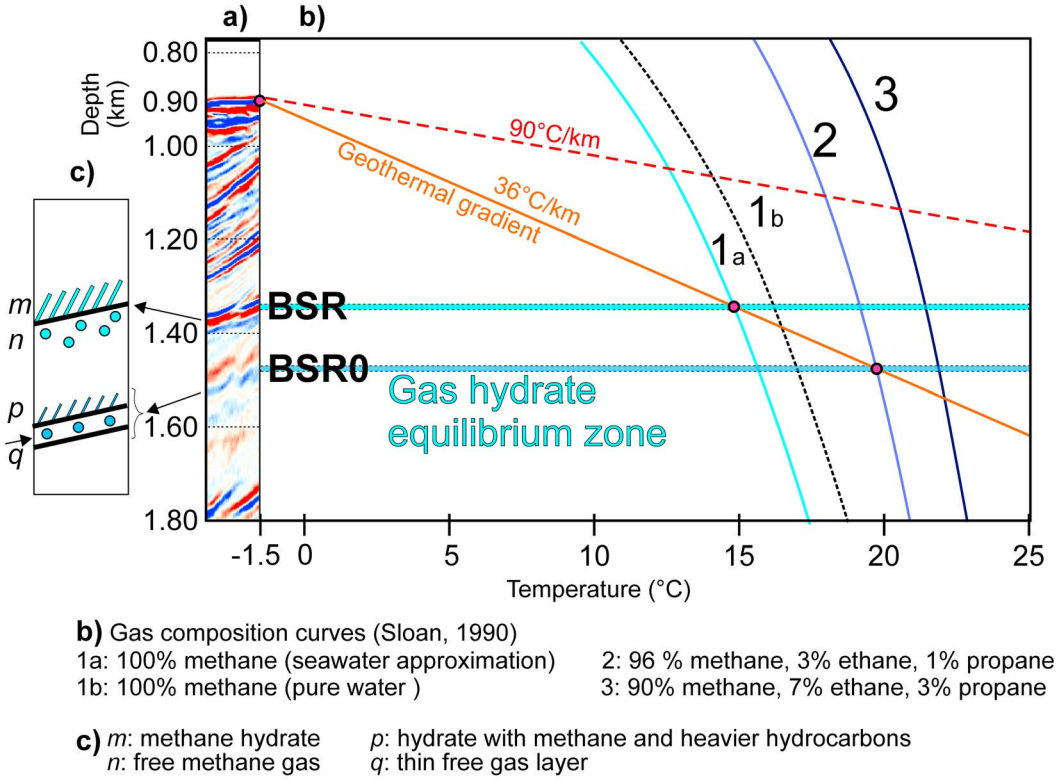

Figure 10. Equilibrium diagram for methane hydrate and for hydrate of varying compositions (curves 1a, 1b, 2 and 3), obtained from the compilation of *Sloan* [1990]. (a) Transect of depth-converted seismic profile IT90AR-63S (see Figure 2c for location), corresponding to the location where the temperature measurements up to 5 m deep sediment were taken [*Della Vedova et al.*, 1992], the seafloor temperature is about −1.5°C [*Della Vedova et al.*, 1992], and water depth is nearly 880 m. (b) The gas hydrate equilibrium zone by the curves with different gas composition [*Sloan*, 1990] and geothermal gradient: in red the average geothermal gradient of 90°C/km from *Della Vedova et al.* [1992] calculated for shallow sediments from the temperature measurements located in Figure 10a, in orange the 36°C/km estimated geothermal gradient assuming the presence of gas hydrate of different composition according to curves 1a (pure methane) and 1b (96% methane plus heavier hydrocarbon) for BSR and BSR0, respectively. The 36°C/km estimated geothermal gradient is similar to those from wells drilled in southern VLB (24–40°C/km). (c) Suggested geological model with the distribution of gas hydrate and free gas of pure methane above and below the BSR and a thin gas layer (q) of 96% methane plus heavier hydrocarbon in correspondence of the BSR0.

3% ethane and 1% propane) for BSR0, the geothermal gradient calculated is about 36°C/km (Figure 10).

5. Discussion

[33] The existence of the BSR indicates the presence of free gas and gas hydrate. The BSR is displaced by the fault strands, where the low-amplitude reflection suggests a gas/fluid and fluidized sediment upward migration (Figures 4 and 9). The gas comes mainly from the free gas-bearing sediment between the BSR and the BSR0. The gas hydrate acts as a trap for the underlying gas, but along fractures/faults the gas can migrate through the shallow sediment up to the seafloor, forming gas seeps and consequently contributing methane to the ocean and potentially to the atmosphere [*MacDonald et al.*, 2002; *Liu and Flemings* 2006; *Mau et al.*, 2006].

[34] The studied data set implies the occurrence of gas hydrate and free gas, not only from the seismic data analysis, but also by the occurrence of gas seeping seafloor morphologies (mud volcanoes and pockmarks), as well as the modeling of the gas hydrate stability zone.

[35] In the stacked profiles, the BSR seismic characteristics, including high amplitude, negative polarity, low frequencies (from 25 Hz above to 20 Hz below the BSR), velocity anomaly (lowering of interval velocity from about 2000 above the BSR to 1400 m/s below), and mimicry of the seafloor topography, are the typical geophysical indicators of the base of gas hydrate and top of free gas.

[36] The frequency field has been investigated by power spectrum panels as a function of time (Figure 4c) and instantaneous frequency sections (Figure 8b). Both attributes show that the BSR has a low-frequency character. The occurrence of free gas below the BSR is associated with the low frequency below the BSR [*Vanneste et al.*, 2002a]. *Wood and Ruppel* [2000], who performed spectral modeling of single-channel seismic and vertical seismic profiling

(VSP) data, showed that attenuation does not occur in the presence of low gas hydrate saturation (3–7% of the pore space), but it is significant in the free gas zone below the BSR. An alternative theory by *Castagna and Sun* [2002], suggesting that the occurrence of free gas provides additional reflected energy at low frequencies, rather than attenuation of higher frequencies, is also consistent with our observations.

[37] Another important indicator of free gas at the BSR interface is the AVO effect [e.g., *Ostrander*, 1984; *Hilterman*, 1990]. In fact, a downward transition to sediment containing free gas, from an overlying sediment without gas, should give negative reflection amplitudes that become larger with increasing offset [e.g., *Minshull and White*, 1989; *Minshull et al.*, 1994; *Andreassen et al.*, 1997; *Carcione and Tinivella*, 2000]. Hence, in the prestack seismic analyses of the BSR (Figures 3 and 5), the negative amplitude increase with offset, according to *Ostrander* [1984] and *Hilterman* [1990], suggests the occurrence of free gas. Moreover, the P wave reflectivity increases with the occurrence of free gas, while the S wave reflectivity depends on the properties of the solid matrix only. Figure 6 shows the BSR and the BSR0 are identified clearly by high-amplitude reflectors in the P wave reflectivity rather than in the S wave reflectivity section where the BSR and BSR0 are imaged weakly. This result is consistent with the occurrence of free gas below the gas hydrate zone.

[38] Where the BSR is strongest, the presence of BSR0 is identified about 120–140 ms in the time-migrated section (80–100 m in the depth conversion) below the BSR. This BSR-BSR0 pairing occurs as parallel horizons, cross-cutting the sedimentary reflectors (Figure 4). The low velocity (a minimum of 1350 m/s between BSR and BSR0 and higher above and below the BSR/BSR0 pair), the high reflection strength, and the low main frequency of about 15–20 Hz (Figures 7 and 8) suggest the presence of free gas. Hence, according to *Andreassen et al.* [2000], the BSR0 could be caused by a thin layer of gas, providing an overall reflection with a positive polarity rather than the reversed polarity of a standard BSR (Figure 10). Alternatively, the lower reflector could be the base of the free gas reflector (BGR), as already suggested by some authors [*Böhm et al.*, 1995; *Lodolo et al.*, 2002; *Posewang and Mienert*, 1999; *Andreassen et al.*, 2000], but in our data, the BGR hypothesis is inconsistent with the base of gas being generally a flat reflection event.

[39] Traversing along the profile, from the basin to the Lee Arch, the BSR evolves into CCRs and EARs. The EARs are seismostratigraphic reflectors related to sediments that likely have higher porosity than the surrounding media, providing a preferential zone for the free gas accumulation [*Judd and Hovland*, 2007]. Similar to the stratigraphy, the EARs could be faulted and tilted, as occurs along the profile IT90A-65 (Figure 7). The top terminations follow the Base of the gas Hydrate Stability Zone (BHSZ), as reported in the Norwegian margin by *Berndt et al.* [2004]. The bottom terminations of the EARs, with changing amplitude, frequency and phase, follow a trend that is deeper and subparallel with the BHSZ (see Figures 2a and 7). An alternate possibility could be that the bottom terminations are determined by how much gas migrates into each reflector.

[40] In the profile IT90A-63, the CCR is located about 200 ms below the seafloor event in the Lee Arch, dipping to about 500 ms below that event, about 3 km westward on the flank (Figure 8). The CCR occurring in the area of active faults could not be identified as a BSR proper because of the depth of the reflectors is offset between each fault segment. As suggested by *Vanneste et al.* [2002b], these offsets can be caused by fluid convection cells which disturb the local gas hydrate stability conditions.

[41] The transition from BSR to CCRs and EARs can be related to transitions in the sediment characteristics, geothermal gradient, and flow behaviors of fluid and gas. Broadly speaking, the BSR proper is present in the less active zone, where pressure, temperature and flow characteristics are laterally homogeneous. On the other hand, the CCRs and EARs are present in the most active area, where faults separate the region into blocks, each with a distinct geothermal gradient, flow characteristics and gas availability. Hence, the stability field of gas hydrates varies from section to section, segmenting the BSR into CCRs and EARs.

[42] Gas/fluid accumulation is elevated in the low-frequency shadow, particularly in the Lee Arch where the tectonic activity is more intense. Moreover, in the Lee Arch, the low frequencies related to the free gas presence appear at shallow depth locations and follow the trend of the CCRs.

[43] Further evidence of gas occurrence is the presence of mud volcanoes, which are necessarily fed by fluids/gas. In this case, the tectonism drives the fluid migration and the mud volcano is built up in correspondence to this flow. A good example is the Tergeste Mud Volcano (Figures 2b and 9) and the mud volcano occurring in the Discovery Graben above the BSR/BSR0 pair (CDP 1300, Figure 4). In both cases the mud volcanoes are fed by chimneys characterized by low seismic amplitude along the conduit, cutting across the stratigraphy down to the BSR/BSR0 pair. On the seafloor, overlying the Lee Arch fault system, pockmarks are also present (Figure 2c). The pockmark features are also found close to this zone [*Lawver et al.*, 2007]. Other reliefs, indicated as mounds in Figures 2a and 2b, have no evidence of gas/fluid escape.

[44] The geophysical evidence of the BSR as the base of gas hydrate stability zone is confirmed by the modeling of the gas hydrate equilibrium (Figure 10). The average geothermal gradient implied by the stability of gas hydrates of different composition, according to the curve of *Sloan* [1990], is about 36°C/km, which would be well within the range of the VLB results. While our multiple composition model is plausible, it is not unique. We use the BSR stability curve assuming pure methane hydrate in seawater (curve 1a in Figure 10b) to derive/calibrate the temperature gradient, which we then use to deduce the composition for BSR0.

6. Conclusions

[45] The targeted reprocessing and prestack analysis of the vintage multichannel seismic reflection data acquired in the Victoria Land Basin (VLB) in 1990 have revealed for the first time in the Ross Sea, the presence of gas hydrate and free gas.

[46] The geophysical evidence from seismic data are (1) the BSR proper, with typical features of a gas-hydrate-related BSR, such as high amplitude and reversed polarity of

the signal, low frequency, crosscutting stratigraphy, and mimicry of the seafloor. It is present in the deeper basin of the Discovery Graben, (2) a second BSR (BSR0) evident locally in the basin about 100 m below the BSR, appearing as a high-amplitude and normal-polarity seismic horizon with a distinct increase of velocity below and crosscutting stratigraphy (the cause of the BSR is most probably the presence of a second stability zone, discarding the base of gas (BGR) hypothesis on the basis of the dipping (nonflat, nonhorizontal) nature of the seismic event), (3) crosscutting reflectors (CCRs), similar to the BSR proper but without mimicking the seafloor, which are present in the western side of the Lee Arch, and (4) enhanced amplitude reflectors (EARs), with negative polarity, low frequency, and high amplitude, which are present in the Lee Arch.

[47] The BSR evolves into CCRs and then to EARs moving along the profile from the basin to the Lee Arch. The distribution of the low frequencies of the seismic reflections, indicating free gas occurrence, forms a "low-frequency shadow" that follows the BSR, CCRs, and EARs.

[48] The BSR/BSR0 pair is identified strongly in the P wave reflectivity sections but only weakly in the S wave section. As the P wave reflectivity increases with the occurrence of free gas, while the S wave reflectivity depends from the properties of the solid matrix only which denotes the occurrence of free gas below the gas hydrate.

[49] The occurrence of free gas in the sediment is also revealed by the presence of mud volcanoes and pockmarks, which are necessarily feed by fluids/gas seeping, mainly migrating upward along faults.

[50] The model for the hydrate stability zone shows that a hydrate-based BSR can exist at the current pressure/temperature conditions. The average geothermal gradient necessary for the BSR and BSR0 to represent the base of hydrate stability is about 36°C/km, which is similar to those for the southern VLB (24–40°C/km).

[51] **Acknowledgments.** The Italian Programma Nazionale di Ricerche in Antartide (PNRA) provided financial support for this work (RIMARS project). We are very grateful to the Associate Editor William Waite for his careful revision and suggestions that allowed us to significantly improve the paper. We thank Josè Carcione for helpful discussion and suggestions for the seismic processing and for reviewing of the manuscript, Bruno Della Vedova and Daniel Praeg for their suggestions on the geothermal model, two anonymous reviewers, Fred Davey, and Nigel Wardell for providing very useful and detailed comments on the manuscript.

References

Andreassen, K., K. Hogstad, and K. A. Berteussen (1990), Gas hydrate in the southern Barents Sea, indicated by a shallow seismic anomaly, *First Break*, *8*(6), 235–245.

Andreassen, K., P. E. Hart, and M. MacKay (1997), Amplitude versus offset modeling of the bottom simulating reflection associated with submarine gas hydrates, *Mar. Geol.*, *137*(1–2), 25–40, doi:10.1016/S0025-3227(96)00076-X.

Andreassen, K., J. Miniert, P. Bryan, and S. C. Singh (2000), A double gas-hydrate related bottom simulating reflector at the Norwegian continental margin, in *Gas Hydrates: Challenges for the Future*, edited by G. D. Holder and P. R. Bishnoi, *Ann. N. Y. Acad. Sci.*, 912, 126–135, doi:10.1111/j.1749-6632.2000.tb06766.x.

Berndt, C., S. Bünz, T. Clayton, J. Mienert, and M. Saunders (2004), Seismic character of bottom simulating reflectors: Examples from the mid-Norwegian margin, *Mar. Pet. Geol.*, *21*(6), 723–733, doi:10.1016/j.marpetgeo.2004.02.003.

Blackman, D. K., R. P. Von Herzen, and L. A. Lawver (1987), Heat flow and tectonics in the western Ross Sea, Antarctica, in *The Antarctic Continental Margin: Geology and Geophysics of the Western Ross Sea*, *Earth Sci. Ser.*, vol. 5B, edited by A. K. Cooper and F. J. Davey, pp. 179–189, Circum-Pac. Counc. of Energy and Miner. Resour., Houston, Tex.

Böhm, G., A. Camerlenghi, E. Lodolo, and A. Vesnaver (1995), Tomographic analysis and geological context of a bottom simulating reflector on the South Shetland Margin (Antarctic Peninsula), *Boll. Geofis. Teor. Appl.*, *37*(145), 3–25.

Bohrmann, G., A. Abelmann, R. Gersonde, H. Hubberton, and G. Kuhn (1994), Pure siliceous ooze, a diagenetic environment for early chert formation, *Geology*, *22*(3), 207–210, doi:10.1130/0091-7613(1994)022<0207:PSOADE>2.3.CO;2.

Brancolini, G., et al. (1995), Seismic stratigraphic atlas of the Ross Sea, Antarctica, in *Geology and Seismic Stratigraphy of the Antarctic Margin*, *Antarct. Res. Ser.*, vol. 68, edited by A. K. Cooper, P. F. Barker, and G. Brancolini, pp. 271–286, 22 plates, AGU, Washington, D. C.

Bucher, G., and E. R. Decker (1976), Down hole temperature measurements in DVDP 15, McMurdo Sound, *Dry Valley Drill. Proj. Bull.*, *7*, 111–112.

Bücker, C. J., T. Wonik, and R. Jarrard (2000), The temperature and salinity profile in CRP-2/2A, Victoria Land Basin, Antarctica, *Terra Antarct.*, *7*(3), 255–259.

Bünz, S., J. Mienert, and C. Berndt (2003), Geological controls on the Storegga gas-hydrate system of the mid-Norwegian continental margin, *Earth Planet. Sci. Lett.*, *209*(3–4), 291–307, doi:10.1016/S0012-821X(03)00097-9.

Cape Roberts Science Team (2000), Studies from the Cape Roberts Project, Ross Sea, Antarctica, initial report on CRP-3, *Terra Antarct.*, *7*(1/2), 1–209.

Carcione, J. M., and S. Picotti (2006), P wave seismic attenuation by slow-wave diffusion: Effects of inhomogeneous rock properties, *Geophysics*, *71*(3), O1–O8, doi:10.1190/1.2194512.

Carcione, J. M., and U. Tinivella (2000), Bottom-simulating reflectors: Seismic velocities and AVO effects, *Geophysics*, *65*(1), 54–67, doi:10.1190/1.1444725.

Castagna, J. P., and S. Sun (2002), The use of spectral decomposition as a hydrocarbon indicator, *GasTIPS, Summer 2002*, 24–27.

Claypool, G. E., T. D. Lorenson, and C. A. Johnson (2003), Authigenic carbonates, methane generation, and oxidation in continental rise and shelf sediments, ODP Leg 188 sites 1165 and 1166, offshore Antarctica (Prydz Bay), *Proc. Ocean Drill. Program Sci. Results*, *188*, 1–15, doi:10.2973/odp.proc.sr.188.004.2003.

Collen, J. D., Y. Xinghua, R. J. Collier, and J. H. Johnston (1989), Hydrocarbon source rock potential and organic maturation, in *Antarctic Cenozoic History From the CIROS-1 Drillhole, McMurdo Sound*, edited by P. J. Barrett, *DSIR Bull. N. Z.*, 245, 223–230.

Cooper, A. K., and P. E. O'Brien (2004), Leg 188 synthesis: Transitions in the glacial history of the Prydz Bay region, East Antarctica, from ODP drilling, *Proc. Ocean Drill. Program, Sci. Results* [online], *188*, doi:10.2973/odp.proc.sr.188.001.2004.

Cooper, A. K., F. J. Davey, and J. C. Behrendt (1987), Seismic stratigraphy and structure of the Victoria Land Basin, Western Ross Sea, Antarctica, in *The Antarctic Continental Margin: Geology and Geophysics of the Western Ross Sea*, *Earth Sci. Ser.*, vol. 5B, edited by A. K. Cooper and F. J. Davey, pp. 27–76, Circum-Pac. Counc. of Energy and Miner. Resour., Houston, Tex.

Davey, F. J. (2004), Ross Sea bathymetry 1:2,000,000, version 1.0, *Geophys. Map 16*, Inst. of Geol. and Nucl. Sci. Ltd., Lower Hutt, New Zealand.

Davies, R. J., and J. Cartwright (2002), A fossilized opal A to opal C/T transformation on the northeast Atlantic margin: Support for a significantly elevated palaeogeothermal gradient during the Neogene?, *Basin Res.*, *14*(4), 467–486, doi:10.1046/j.1365-2117.2002.00184.x.

Della Vedova, B., G. Pellis, L. A. Lawver, and G. Brancolini (1992), Heat-flow and tectonics of the western Ross Sea, in *Recent Progress in Antarctic Earth Science, Proceedings of the Sixth International Symposium on Antarctic Earth Science, Ranzan, Saitama, Japan, September 9–13, 1991*, edited by Y. Yoshida, K. Kaminuma, and K. Shiraishi, pp. 627–637, Terra Sci., Tokyo.

Domenico, S. N. (1977), Elastic properties of unconsolidated porous sand reservoirs, *Geophysics*, *42*(7), 1339–1368, doi:10.1190/1.1440797.

Foucher, J. P., H. Nouzé, and P. Henry (2002), Observation and tentative interpretation of a double BSR on the Nankai slope, *Mar. Geol.*, *187*(1–2), 161–175, doi:10.1016/S0025-3227(02)00264-5.

Gei, D., and J. M. Carcione (2003), Acoustic properties of sediments saturated with gas hydrate, free gas and water, *Geophys. Prospect.*, *51*(2), 141–158, doi:10.1046/j.1365-2478.2003.00359.x.

Hein, J. R., D. W. Scholl, J. A. Barron, M. G. Jones, and J. Miller (1978), Diagenesis of late Cenozoic diatomaceous deposits and formation of the

bottom simulating reflector in the southern Bering Sea, *Sedimentology*, *25*(2), 155–181, doi:10.1111/j.1365-3091.1978.tb00307.x.

Hilterman, F. (1990), Is AVO the seismic signature of lithology? A case history of Ship Shoal-south addition, *Leading Edge*, *9*(6), 15–22, doi:10.1190/1.1439744.

Hyndman, R., and G. Spence (1992), A seismic study of methane hydrate marine bottom simulating reflectors, *J. Geophys. Res.*, *97*(B5), 6683–6698, doi:10.1029/92JB00234.

Judd, A., and M. Hovland (2007), *Seabed Fluid Flow. The Impact on Geology, Biology and the Marine Environment*, 492 pp., Cambridge Univ. Press, Cambridge, U. K.

Kvenvolden, K. A., and A. K. Cooper (1987), Natural gas hydrates of the offshore Circum-Pacific Margin—A future energy resource?, in *Transactions of the 4th Circum-Pacific Energy and Mineral Resource Conference*, edited by M. K. Horn, pp. 285–297, Circum-Pac. Counc. for Energy and Miner. Resour., Houston, Tex.

Kvenvolden, K. A., M. Golan-Bac, and J. B. Rapp (1987), Hydrocarbon geochemistry of sediments offshore from Antarctica: Wilkes Land continental margin, in *The Antarctic Continental Margin: Geology and Geophysics of Offshore Wilkes Land*, *Earth Sci. Ser.*, vol. 5A, edited by S. L. Eittreim and M. A. Hampton, pp. 205–213, Circum-Pac. Counc. of Energy and Miner. Resour., Houston, Tex.

Lawver, L. A., M. B. Davis, and T. J. Wilson, and the Shipboard Scientific Party (2007), Neotectonic and other features of the Victoria Land Basin, Antarctica, interpreted from multibeam bathymetry data, in *Antarctica: A Keystone in a Changing World—Online Proceedings for the 10th International Symposium on Antarctic Earth Sciences, Santa Barbara, California, U.S.A.—August 26 to September 1, 2007*, edited by A. Cooper, C. Raymond, and the 10th ISAES Editorial Team, *U.S. Geol. Surv. Open File Rep.*, *2007-1047*, EA 017, 4 pp.

Liu, X., and P. B. Flemings (2006), Passing gas through the gas hydrate stability zone at southern Hydrate Ridge, offshore Oregon, *Earth Planet. Sci. Lett.*, *241*(1–2), 211–226, doi:10.1016/j.epsl.2005.10.026.

Lodolo, E., A. Camerlenghi, and G. Brancolini (1993), A bottom simulating reflector on the South Shetland margin, Antarctic Peninsula, *Antarct. Sci.*, *5*(02), 207–210, doi:10.1017/S0954102093000264.

Lodolo, E., A. Camerlenghi, G. Madrussani, U. Tinivella, and G. Rossi (2002), Assessment of gas hydrate and free-gas distribution on the South Shetland margin (Antarctica) based on multichannel seismic reflection data, *Geophys. J. Int.*, *148*(1), 103–119, doi:10.1046/j.0956-540x.2001.01576.x.

Lonsdale, M. J. (1990), The relationship between silica diagenesis, methane, and seismic reflections on the South Orkney microcontinent, *Proc. Ocean Drill. Program Sci. Results*, *113*, 27–36, doi:10.2973/odp.proc.sr.113.177.1990.

MacDonald, I. R., I. Leifer, R. Sassen, P. Stine, R. Mitchell, and N. J. Guinasso (2002), Transfer of hydrocarbons from natural seeps to the water column and atmosphere, *Geofluids*, *2*(2), 95–107, doi:10.1046/j.1468-8123.2002.00023.x.

Markl, R. G., G. M. Bryan, and J. I. Ewing (1970), Structure of the Blake-Bahama Outer Ridge, *J. Geophys. Res.*, *75*(24), 4539–4555, doi:10.1029/JC075i024p04539.

Mau, S., H. Sahling, G. Rehder, E. Suess, P. Linke, and E. Soeding (2006), Estimates of methane output from mud extrusions at the erosive convergent margin off Costa Rica, *Mar. Geol.*, *225*(1–4), 129–144, doi:10.1016/j.margeo.2005.09.007.

McIver, R. D. (1975), Hydrocarbon gases in canned core samples from Leg 28 sites 271, 272, and 273, Ross Sea, *Initial Rep. Deep Sea Drill. Proj.*, *28*, 815–817, doi:10.2973/dsdp.proc.28.128.1975.

Mienert, J., J. Posewang, and D. Lukas (2001), Changes in the hydrate stability zone on the Norwegian margin and their consequence for methane and carbon releases into the oceanosphere, in *The Northern North Atlantic: A Changing Environment*, edited by P. Schäfer, et al., pp. 259–280, Springer, Berlin.

Minshull, T., and R. White (1989), Sediment compaction and fluid migration in the Makran accretionary prism, *J. Geophys. Res.*, *94*(B6), 7387–7402, doi:10.1029/JB094iB06p07387.

Minshull, T., S. Singh, and G. Westbrook (1994), Seismic velocity structure at a gas hydrate reflector, offshore western Colombia, from full waveform inversion, *J. Geophys. Res.*, *99*(B3), 4715–4734, doi:10.1029/93JB03282.

Ostrander, W. F. (1984), Plane-wave reflection coefficients for gas sands at nonnormal angles of incidence, *Geophysics*, *49*(10), 1637–1648, doi:10.1190/1.1441571.

Posewang, J., and J. Mienert (1999), The enigma of double BSRs: Indicators for changes in the hydrate stability field?, *Geo Mar. Lett.*, *19*(1–2), 157–163, doi:10.1007/s003670050103.

Rapp, J. B., K. A. Kvenvolden, and M. Golan-Bac (1987), Hydrocarbon geochemistry of sediments offshore from Antarctica, in *The Antarctic Continental Margin: Geology and Geophysics of the Western Ross Sea*, *Earth Sci. Ser.*, vol. 5B, edited by A. K. Cooper and F. J. Davey, pp. 217–224, Circum-Pac. Counc. of Energy and Miner. Resour., Houston, Tex.

Rebesco, M., R. D. Larter, P. F. Barker, A. Camerlenghi, and L. E. Vanneste (1997), The history of sedimentation on the continental rise west of the Antarctic Peninsula, in *Geology and Seismic Stratigraphy of the Antarctic Margin, Part 2*, *Antarct. Res. Ser.*, vol. 71, edited by P. F. Barker and A. K. Cooper, pp. 29–49, AGU, Washington, D. C.

Rossetti, F., F. Storti, M. Busetti, F. Lisker, G. Di Vincenzo, A. Läufer, S. Rocchi, and F. Salvini (2006), Eocene initiation of Ross Sea dextral faulting and implications for East Antarctic neotectonics, *J. Geol. Soc.*, *163*(1), 119–126, doi:10.1144/0016-764905-005.

Salvini, F., G. Brancolini, M. Busetti, F. Storti, F. Mazzarini, and F. Coren (1997), Cenozoic geodynamics of the Ross Sea region, Antarctica: Crustal extension, intraplate strike-slip faulting, and tectonic inheritance, *J. Geophys. Res.*, *102*(B11), 24,669–24,696, doi:10.1029/97JB01643.

Shipley, T. H., M. N. Houston, R. T. Buffler, F. S. Shaub, K. S. McMillen, J. W. Ladd, and J. L. Worzel (1979), Seismic reflection evidence for the widespread occurrence of possible gas-hydrates horizons on continental slopes and rises, *AAPG Bull.*, *63*(12), 2204–2213.

Sissons, B. A. (1980), Down hole temperatures, in *Immediate Report of VUWAE 24 and McMurdo Sound Sediment and Tectonic Studies (MSSTS)*, edited by A. Pyne and D. B. Waghorn, p. 14, Victoria Univ. of Wellington, Wellington.

Sloan, E. D. (1990), *Clathrate Hydrates of Natural Gases*, 1st ed., 641 pp., Marcel Dekker, New York.

Stewart, R. R. (1990), Joint P and P-SV inversion, *CREWES Res. Rep. 2*, Consortium for Res. in Elastic Wave Explor. Seismol., Calgary, Alberta, Canada.

Taner, M. T., and R. E. Sheriff (1977), Application of amplitude, frequency and other attributes to stratigraphy and hydrocarbon exploration, in *Seismic Stratigraphy: Applications to Hydrocarbon Exploration*, edited by C. E. Payton, *AAPG Mem.*, *26*, 301–327.

Taner, M. T., F. Koehler, and R. E. Sheriff (1979), Complex seismic trace analysis, *Geophysics*, *44*(6), 1041–1063, doi:10.1190/1.1440994.

Taner, M. T., J. S. Schuelke, R. O'Doherty, and E. Baysal (1994), Seismic attributes revisited, paper presented at 64th Annual International Meeting, Soc. of Explor. Geophys., San Antonio, Tex.

Taylor, M. H., W. P. Dillon, and I. A. Pecher (2000), Trapping and migration of methane associated with the gas hydrate stability zone at the Blake Ridge Diapir: New insights from seismic data, *Mar. Geol.*, *164*(1–2), 79–89, doi:10.1016/S0025-3227(99)00128-0.

Tinivella, U., and F. Accaino (2000), Compressional velocity structure and Poisson's ratio in marine sediments with gas hydrate and free-gas by inversion of reflected and refracted seismic data (South Shetland Islands, Antarctica), *Mar. Geol.*, *164*(1–2), 13–27, doi:10.1016/S0025-3227(99)00123-1.

Tinivella, U., E. Lodolo, A. Camerlenghi, and G. Böhm (1998), Seismic tomography study of a bottom simulating reflector off the South Shetland Islands (Antarctica), in *Gas Hydrate: Relevance to World Margin Stability and Climate Change*, edited by J. P. Henriet and J. Mienert, *Geol. Soc. Spec. Publ.*, *137*, 141–151, doi:10.1144/GSL.SP.1998.137.01.11.

Vanneste, M., J. Mienert, S. Guidard, and HYDRATECH-INGGAS Partners (2002a), "Arctic" gas hydrates offshore Western Svalbard, Norway, in *Proceedings of the 4th International Conference on Gas Hydrates*, edited by Y. H. Mori, pp., 222–227, Int. Conf. on Gas Hydrates, Yokohama, Japan.

Vanneste, M., J. Poort, M. De Batist, and J. Klerkx (2002b), Atypical heat-flow near gas hydrate irregularities and cold seeps in the Baikal Rift Zone, *Mar. Pet. Geol.*, *19*(10), 1257–1274, doi:10.1016/S0264-8172(03)00019-9.

Volpi, V., A. Camerlenghi, C. D. Hillenbrandt, M. Rebesco, and R. Ivaldi (2003), Effect of biogenic silica on sediment compaction and slope stability on the Pacific margin of the Antarctic Peninsula, *Basin Res.*, *15*(3), 339–363, doi:10.1046/j.1365-2117.2003.00210.x.

White, P. (1989), Downhole logging, in *Antarctic Cenozoic History From the CIROS-1 Drillhole McMurdo Sound*, edited by P. J. Barrett, *DSIR Bull. N. Z.*, *245*, 7–14.

Wood, W. T., and C. Ruppel (2000), Seismic and thermal investigations of the Blake Ridge gas hydrate area: A synthesis, *Proc. Ocean Drill. Program Sci. Results*, *164*, 253–264, doi:10.2973/odp.proc.sr.164.203.2000.

Yilmaz, Ö. (2001), *Seismic Data Analysis: Processing, Inversion, and Interpretation of Seismic Data*, *Invest. Geophys.* 10(1/2), edited by M. R. Cooper, 2027 pp., Soc. of Explor. Geophys., Tulsa, Okla.

M. Busetti and R. Geletti, Istituto Nazionale di Oceanografia e di Geofisica Sperimentale, Borgo Grotta Gigante 42/c, I-34010 Sgonico (TS), Italy. (rgeletti@inogs.it)